Late Holocene tephrostratigraphy from Cajas National Park, southern Ecuador

*Stéphanie H. Arcusa[1], Tobias Schneider[2,3], Pablo V. Mosquera[4,5], Hendrik Vogel[6], Darrell Kaufman[1], Sönke Szidat[7], Martin Grosjean[3]

[1] *School of Earth and Sustainability, Northern Arizona University, PO Box 4099, Flagstaff, AZ 86011-4099, USA.*
   sha59@nau.edu; darrell.kaufman@nau.edu

[2] *Department of Geosciences, Morrill Science Center, University of Massachusetts, 611 North Pleasant Street, Amherst, MA 01003, USA.*
   tobias.schneider@giub.unibe.ch

[3] *Institute of Geography and Oeschger Centre for Climate Change Research, University of Bern, Hallerstrasse 12, 3012 Bern, Switzerland.*
   martin.grosjean@oescher.unibe.ch

[4] *Subgerencia de Gestión Ambiental, Empresa Pública Municipal de Telecomunicaciones, Agua potable, Alcantarillado y Saneamiento (ETAPA EP), Benigno Malo 7-78, Cuenca EC010101, Ecuador.*
   pmosquerav@gmail.com

[5] *Departament de Biologia Evolutiva, Ecologia i Ciències Ambientals, Universitat de Barcelona, Diagonal 643, 08028 Barcelona, Spain.*

[6] *Institute of Geological Sciences and Oeschger Center for Climate Change Research, University of Bern, Baltzerstrasse 3, 3012 Bern, Switzerland.*
   hendrik.vogel@geo.unibe.ch

[7] *Department of Chemistry and Biochemistry and Oeschger Centre for Climate Change Research, University of Bern, Baltzerstrasse 3, 3012 Bern, Switzerland.*
   szidat@dcb.unibe.ch

*Corresponding author: sha59@nau.edu

ABSTRACT. Lakes located downwind of active volcanoes serve as a natural repository for volcanic ash (tephra) produced during eruptive events. In this study, sediment cores from four lakes in Cajas National Park, southern Ecuador, situated approximately 200 km downwind of active volcanoes in the Northern Andes Volcanic Zone, were analysed to document the regional history of tephra fall extending back around 3,000 a cal BP. The ages of the lacustrine sedimentary sequences were constrained using a total of 20 AMS radiocarbon ages on plant remains. The tephra layers were correlated among the lakes based on their radiocarbon age, elemental composition, colour, and grain morphology. We found five unique tephra layers, each at least 0.2 cm thick, and further constrained their ages by combining the results from two age-depth modelling approaches (clam and rbacon). The tephra layers were deposited 3,034±621, 2,027±41, 1,557±177, 733±112, and 450±70 a cal BP. The ages of all but the youngest tephra layer overlap with those of known eruptions from Tungurahua. Some tephra layers are missing as macroscopic layers in several cores, with only two of the five tephra layers visible in the sediment of three lakes. Likewise, previous studies of lake sediment cores from the region are missing the four youngest tephra layers, further highlighting the need to sample multiple lakes to reconstruct a comprehensive history of fallout events. The newly documented stratigraphic marker layers will benefit future studies of lake sediments in Cajas National Park.

Keywords: Tephra, Taphonomy, Tephra morphology, Radiocarbon, ^{14}C chronology, Limnogeology, Andes, South America.

RESUMEN. Tefroestratigrafía del Holoceno Tardío, Parque Nacional Cajas, Ecuador. Lagos que están localizados en la trayectoria del viento que proviene desde volcanes activos, sirven como repositorios naturales de cenizas volcánicas (tefra) producidas durante eventos eruptivos. En este estudio, se analizaron testigos de sedimentos obtenidos en sondajes realizados en cuatro lagos del Parque Nacional Cajas, en el sur de Ecuador, situados aproximadamente a 200 km de volcanes activos en la Zona Volcánica Norte de los Andes. El objetivo del estudio es documentar la historia regional de la deposición de tefras ocurrida en los últimos 3.000 años. Las edades de las secuencias sedimentarias lacustres fueron definidas con un total de 20 edades de radiocarbono AMS realizadas en restos de plantas fosilizados. Los niveles de tefras fueron correlacionados entre los lagos sobre la base de su edad de radiocarbono, color y morfología de grano. Se identificaron cinco niveles de tefras, cada uno de al menos 0,2 cm de espesor, y sus edades fueron adicionalmente restringidas con los resultados provenientes de dos modelos de edad-profundidad (clam y rbacon) aplicados a las secuencias sedimentarias. Las tefras fueron depositadas a 3.034±621, 2.027±41, 1.557±177, 733±112, y 450±70 a cal AP. Las edades de todas, menos la de la capa de tefra más joven, se superponen con las de erupciones conocidas del volcán Tungurahua. En varios de los testigos de sedimentos los niveles de tefras no son visibles como capas macroscópicas, solamente dos de los cinco niveles de tefra identificados eran observables en la secuencia sedimentaria de tres de los lagos. Estudios previos de testigos de sedimento lacustre realizados en la región no registraron la presencia de los cuatro niveles de tefras más jóvenes, lo que realza la necesidad de muestrear múltiples lagos para reconstruir una historia completa de eventos de deposición de ceniza volcánica originada por eventos eruptivos. Las capas de tefras recién documentadas consituyen marcadores estratigráficos que beneficiarán futuros estudios de sedimentos lacustres en el Parque Nacional Cajas.

Palabras clave: Tefra, Tafonomía, Morfología de tefra, Radiocarbono, Cronología ^{14}*C, Limnogeología, Andes, América del Sur.*

1. Introduction

Tephrochronology is increasingly useful in Quaternary paleoenvironmental research. Tephra beds record explosive volcanic eruptions extending back beyond direct observations in a region. This is fundamental for risk assessments based on eruption frequencies and magnitudes as inferred from long (*e.g*., Holocene) tephrochronological time series (Alloway *et al*., 2013). Furthermore, tephra layers serve as chronostratigraphic markers that are deposited simultaneously over extensive areas and in a variety of terrestrial and aquatic settings. Such markers are useful to evaluate and improve chronologies of sedimentary successions, including those recovered from lakes (Lowe, 2011).

Developing tephrochronologies from lakes using sedimentary records can be challenging. Different methods of tephra analysis including geochemistry, colour, grain morphology, and stratigraphy can yield conflicting results (Shane, 2000; Zawalna-geer *et al*., 2016). Additionally, multiple variables influence the completeness of a tephra fall sequence at a site. For example, wind direction, secondary deposition, reworking, dissolution, and narrow plumes can generate variable tephra stratigraphic records (*e.g*., Boygle, 1999; De Fontaine *et al*., 2007). To address the issue of heterogeneous areal deposition a multi-lake approach with multiple sediment cores is needed for a comprehensive account of tephra fall events.

Of the 20 active volcanoes in Ecuador (Hall *et al*., 2008), many have experienced disruptive to devastating historical eruptions (Fig. 1A; Venzke, 2016) but less is known about pre-historic eruptions. Holocene tephrochronologies have been developed from several sites in Ecuador (*e.g.,* Garrison *et al*., 2011; Hall *et al*., 1999; Hidalgo *et al*., 2008; Le Pennec *et al*., 2012; Monzier *et al*., 1999; Mothes and Hall, 2008) although only one from the southern part of the country (Rodbell *et al*., 2002) and none focusing on the past several thousand years (late Holocene).

Hundreds of lakes in Cajas National Park (CNP) occur on the eastern slope of the western Cordillera of south-central Ecuador (Mosquera *et al*., 2017). They likely received tephra fall from explosive volcanism throughout the Quaternary making CNP an attractive location from which to produce a tephrostratigraphy. Although the prevailing winds are easterly and volcanoes are located north of the park, the park is close to several active volcanoes (Fig. 1A). Previous work in the park revealed seven Holocene tephra deposits, yet none during the last 2,000 years (Rodbell *et al*., 2002, 2008). This is unexpected because at least 34 late Holocene eruptions with Volcanic Eruption Index (VEI) ≥4 have occurred in Ecuador, some from volcanoes like Tungurahua, which is located within 200 km to the north of the park (Venzke, 2016).
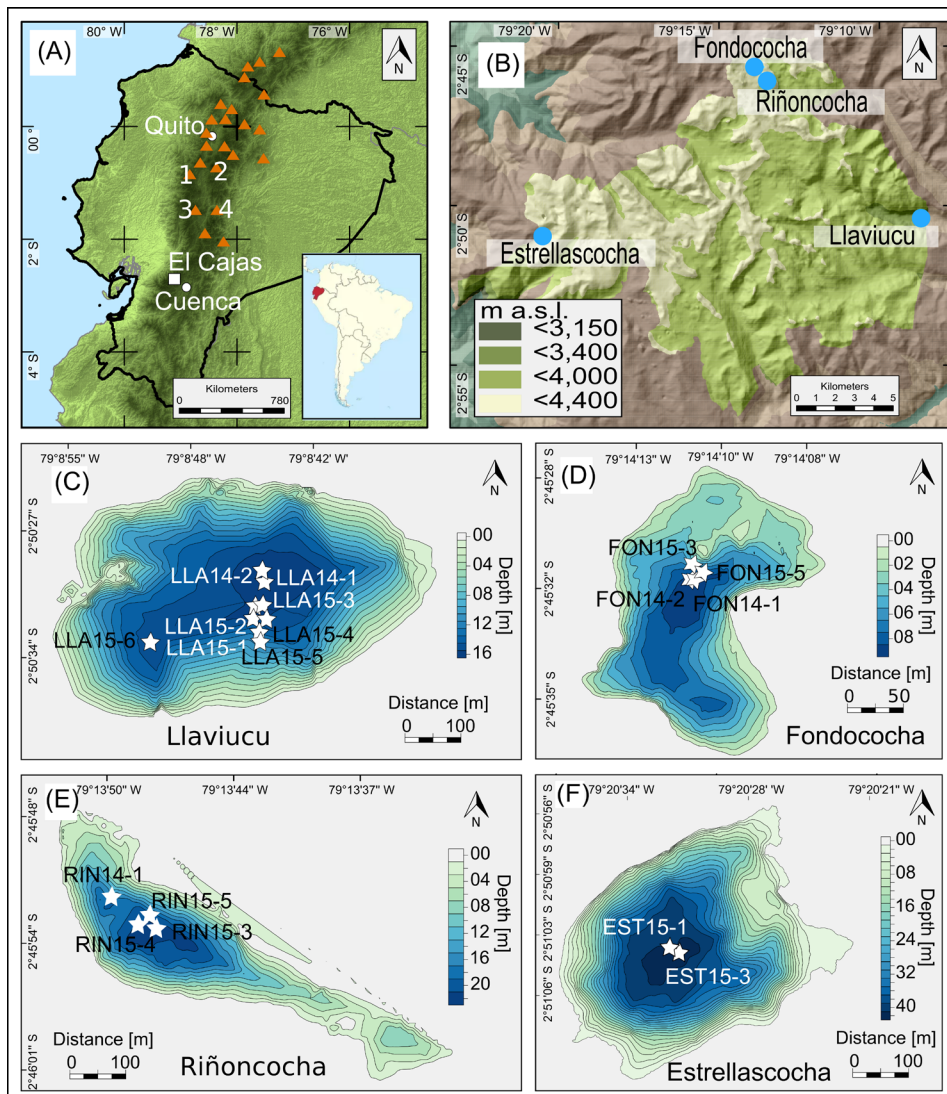
FIG. 1. Study site. **A.** Ecuador showing El Cajas National Park, southern Ecuador, in relation to active volcanoes (triangles) (Venzke, 2016). Volcano **1:** Quilotoa, **2:** Cotopaxi, **3:** Chimborazo, and **4:** Tungurahua. Inset in (**A**) shows the location of Ecuador in South America. **B.** El Cajas National Park (green area) showing the locations of Lakes Llaviucu, Fondococha, Riñoncocha, and Estrellascocha (blue dots) and the elevation gradient. Bathymetry maps for Lakes Llaviucu **(C)**, Fondococha **(D)**, Riñoncocha **(E)**, and Estrellascocha **(F)**, showing the coring locations (asterisks).

In this study, we develop a tephrostratigraphy of the last 3,000 years using a multi-lake, multi-core approach in CNP, southern Ecuador. Radiocarbon dating, with supporting evidence from tephra colour, and grain morphology are used to distinguish and date five regionally distributed late Holocene marker layers. This study also points to challenges using lake sediments to establish tephrostratigraphy in this type of environment.

2. Study Area and Previous Work

Cajas National Park (CNP, S 79°10' W, Fig. 1A, B) is located in southern Ecuador and ranges from 3,150 m to 4,400 m a.s.l. Bedrock consists mainly of andesite, rhyolite, and tuff of the Pleistocene Tarqui Formation (Paladines and Guzmán, 1980). The landscape is covered with Holocene Andosols and Histosols (Buytaert *et al*., 2006; Harden, 2006)

and hosts 218 lakes of glacial origins (Van Colen *et al.*, 2017) and over 5,000 water bodies (Mosquera *et al.*, 2017).

Because heterogeneous areal distribution of tephra deposition affects all lakes, sampling of lakes in a variety of settings allows us to define a more complete tephrostratigraphy for the area. We selected four lakes located closely (<20 km) one to another, but in different settings (Table 1). Lakes Llaviucu, Fondococha, Riñoncocha, and Estrellascocha are four exorheic high-altitude lakes in CNP (Fig. 1B-F) arranged E-W along an elevation gradient of *ca*. 1,000 m. Their catchment characteristics differ in slope steepness, vegetation type, and catchment-to-lake area ratio (Table 1).

Previous research on tephrochronology using lake sediments in CNP is limited to one published study. Rodbell *et al.* (2002) developed the first tephrochronology for this area based on Lake Llaviucu and five other lakes, and they identified seven late-glacial and Holocene tephra layers (A-G, Rodbell *et al.*, 2002). The youngest of these tephra layers dates to *ca*. 4,100 a cal BP in Lake Llaviucu, which is geochemically correlated to the uppermost tephra layer in Lake Chorreras (dated to *ca*. 3,400 a cal BP) and to the uppermost tephra layer in Lake Pallcacocha (F, G dated to 3,380 and 4,430 a cal BP, respectively). Thus, the age of the youngest tephra layer identified up to now is relatively poorly constrained (Rodbell *et al.*, 2002), and these authors also noted the absence of tephra

layers for the past two millennia. For their study on late Holocene clastic event layers, Schneider *et al.* (2018) established a first radiocarbon (^{14}C) chronology for Lake Fondococha and found that ^{14}C dating of these lake sediments is challenging because sediment organic matter is strongly decomposed, terrestrial macrofossils are scarce, and bulk sediment organic matter is affected by ^{14}C reservoir effects.

3. Methods

3.1. Coring, sediment description and non-destructive methods

Sediment cores were retrieved from the four lakes in 2014 and 2015 (core ID names identified as 14 and 15, respectively) using a gravity coring system with percussion hammer (6 cm diameter, UWITEC, Austria) operated from a rubber raft. Between two and six cores, each between 50- and 195 cm long were obtained from or near the depocenter of the lakes (Fig. 1C-F). The sediment surfaces were preserved using wet floral foam. The sediment cores were shipped to the University of Bern, Switzerland and stored in the dark at 4 °C until analysis. The sealed whole cores were first scanned for magnetic susceptibility (MS) and gamma-ray-inferred density with a Multi-Sensor Core Logger (MSCL, Geotek; Schultheiss and Weaver, 1992) at 1 cm resolution. The cores were then split, and the sediment was described after Schnurrenberger *et al.* (2003). Colour was identified

TABLE 1. LAKE AND CATCHMENT CHARACTERISTICS FOR LAKES LLAVIUCU, FONDOCOCHA, RIÑONCOCHA, AND ESTRELLASCOCHA.

Parameters	Llaviucu	Fondococha	Riñoncocha	Estrellascocha
Lat. (S)	2° 50' 35.5194"	2° 45' 35.2794"	2° 45' 59.0394"	2° 51' 7.9194"
Lon. (W)	79° 8' 45.96"	79° 14' 11.04"	79° 13' 46.9194"	79° 20' 31.56"
Elev. (m a.s.l.)	3,152	4,127	4,034	4,128
Max. depth (m)	16.5	9.9	29.6	41.6
LA (km^2)	0.19	0.03	0.1	0.12
CA (km^2)	47.70	0.6	3.87	1.46
CA/LA	253	18	6	12
Vegetation community	Pasture grassland/montane, Andean forest	Paramo/sub-paramo	Paramo/sub-paramo	Paramo/sub-paramo
Trophic state	Mesotrophic	Oligotrophic	Oligotrophic	Oligotrophic

Lat: latitude; **Lon:** longitude; **Elev:** elevation; **LA:** lake area; **CA:** catchment area.
Information from Mosquera *et al.* (2017).

following Munsell's colour chart. A micro X-Ray Fluorescence (µXRF) scanner (ITRAX©, Cox Analytical System) was used to measure the elemental composition (Croudace *et al*., 2006) at a resolution of 2 mm for the 2014 half cores and 1 mm increments for the 2015 half cores to detect tephra layers and cryptotephra-bearing horizons (Vogel *et al*., 2010). The 2014 split cores were measured using a Mo tube (40 kV, 20 mA) with 10 s exposure time to detect Al, Si, K, Ca, Ti, Mn, Fe, Rb, S, Sr, and Zr. The 2015 split cores were measured with higher voltage (45 kV) and longer exposure (20 s) to detect additional elements (Ni, Cu, Pb, Br). The split cores were additionally imaged using X-Ray Radiography (RAD, 0.2 mm resolution) to detect differences in the sediment density at high resolution. Core-face photographs (visible and near infrared) were acquired using a SPECIM Ltd. VNIR hyperspectral imaging scanning system (Butz *et al*., 2015). In cores from Lake Fondococha, clastic event layers related to high runoff were previously determined by Schneider *et al*. (2018) using Principal Component Analysis (PCA) of elemental compositions and visual inspection. Organic-rich debris and clastic layers were mapped visually in Lake Llaviucu and interpreted as rapidly deposited event deposits.

3.2. Tephra layer identification

This study focuses on the visually prominent, relatively pure tephra beds and some cryptotephra, disseminated tephra shards that are not macroscopically obvious. Samples from tephra layers that could be easily correlated among cores from the same lake were combined to increase the mass of relatively pure tephra sample. Tephra layers were distinguished from the ambient lacustrine sediment by their brighter colour, higher MS, higher Sr and Si abundances (Vogel *et al*., 2010), low RAD, and presence of relatively angular glass shards as visualised through light microscopy and Scanning Electron Microscopy (SEM). Zones of higher Sr and Si abundances were investigated for cryptotephra using smear slides. The size and shape of tephra grains were analysed from SEM images using the modified method of Liu *et al*. (2016). Grain-size was not used to assess componentry. Additionally, elemental composition for each macro tephra layer was obtained from µXRF (*e.g*., Vogel *et al*., 2010; Kylander *et al*., 2012; Peti *et al*., 2019). PCA was used to aid correlation

among tephra beds by visualising the distribution of the samples' elemental composition in a low-dimensional space.

3.3. Tephra layer age determination

Lake sediments were sampled contiguously and wet sieved (120 µm mesh, 0.5-1.0 cm intervals) to recover terrestrial plant remains. As identifiable terrestrial plant remains were scarce, we also performed parallel ^{14}C AMS measurements on the bulk sediment to assess whether these materials yield reliable ^{14}C ages or are affected by ^{14}C reservoir effects (Geyh *et al*., 1999). Plant remains were identified and taxonomically classified under dissecting microscope and dated with a ^{14}C AMS MIni-CArbon DAting System (MICADAS) at the University of Bern (Szidat *et al*., 2014). The smallest samples (<100 µg carbon) were analysed with direct gas injection (Salazar *et al*., 2015); larger samples were analysed following conversion to graphite. All ^{14}C ages were calibrated to calendar years using the IntCal13 northern hemisphere calibration (Reimer *et al*., 2013) because CNP is located within the South American Summer Monsoon region and thus is strongly influenced by the northern hemisphere air masses (Marsh *et al*., 2018).

The age-depth model for Lake Llaviucu was constrained by 12 new AMS ^{14}C ages on plant remains from two parallel cores mapped onto a composite (supplementary Fig. S1) and is presented here for the first time. The ^{210}Pb activity profiles from the near-surface sediment of Lakes Fondococha and Llaviucu were previously presented in Bandowe *et al*. (2018). The age-depth model for Lake Fondococha was initially developed by Schneider *et al*. (2018) and is complemented here with additional ^{14}C dates to better constrain the ages of the tephra layers.

These age-depth models were used to date the tephra layers in cores from Lakes Llaviucu and Fondococha. Due to the lack of suitable material, ^{14}C chronologies could not be established for Lakes Riñoncocha and Estrellascocha. In these lakes, no identifiable terrestrial plant remains could be found, despite extensive sediment sieving (63 µm mesh). The age assigned to each tephra bed in this study was based on the two lakes with age-depth models. In addition, we compared the results of two commonly applied age-depth modelling routines, namely clam v.2.3.2 (Blaauw, 2019) and rbacon v.2.3.9.1 (Blaauw and Christen, 2019), both available for the open-

source statistical software "R" (R Core Team, 2019) (supplementary Table S1). Each model for each lake yielded tephra layer ages and uncertainty, for a total of four age estimates per tephra layer (two lakes and two models per lake). The best age estimates for each tephra layer were calculated as the mean age at the base of the tephra layer bed as represented by the four age estimates, with each age weighted by the inverse of the one-sigma range of the uncertainty (supplementary Table S2). The age uncertainty was calculated as the root mean squared error (RMSE) based on the uncertainties of the four age estimates. Pure tephra beds and clastic-rich layers interpreted as flood deposits (identified based on datasets described below) were considered instantaneous and therefore removed from the age-depth models (supplementary Table S3).

4. Results

4.1. Sediment stratigraphy

The sediment in Lake Llaviucu is composed of brownish black (HUE 10YR3/1) organic-rich silt with layers of plant remains interspersed with olive yellow (HUE 5Y6/4) to greyish olive (HUE 7.5YR6/2) laminae. Sediment from Lake Fondococha was previously described as brownish black (HUE 10YR2/1) organic-rich, laminated silty clay (Schneider *et al.*, 2018; Fig. 2). Similarly, the sediment of Lake Riñoncocha consists of a pink (HUE 7.5YR8/3), thinly laminated clay section (110-130 cm sediment depth) overlain by yellowish brown (HUE 10YR5/4) thinly laminated silty clay that progressively grades upward to brownish black (HUE 10YR2/1) massive sediment. The sediment consists of strongly decomposed organic matter, diatom ooze, and siliciclastic volcanic material. Unlike the other lakes, Lake Estrellascocha's sediment consists of brown (HUE 10YR5/3), massive silty clay derived from volcanic siliciclastic rocks, and comprises strongly decomposed organic matter and diatom ooze.

The prominent mm- to cm-thick, normally graded, silty-clay beds found in cores from Lake Fondococha were previously interpreted as flood-deposited sediments (Schneider *et al.*, 2018). In Lake Llaviucu, the layers are also normally graded, and their origin is interpreted similarly in this study.

Cores collected from nearby sites in 2014 and 2015 were readily correlated based on prominent tephra layers in Lakes Fondococha and Riñoncocha (supplementary Fig. S1), but three visible tephra layers were missing from some of the cores. The youngest tephra layer found in Lake Llaviucu is missing in LLA14-1, the oldest tephra layer found in Lake Fondococha is missing from FON15-5, and the two oldest tephra layers found in Lake Estrellascocha are missing in EST15-1. However, we did not explicitly search for cryptotephra at the depths where they should have been located. Correlation using MS and µXRF data between multiple cores from Lake Llaviucu proved more challenging due to the abundance of clastic sediment layers but led to the conclusion that 22 cm of sediment was missing in core LLA15-6 (supplementary Fig. S1). A master sediment core composite for Lake Llaviucu was constructed from cores LLA14-1, LLA14-2, and LLA15-6.

4.2. Age-depth models

Twenty AMS ^{14}C ages distributed between Lakes Llaviucu and Fondococha were used to develop age-depth models (Table 2, Fig. 3). The 12 ages from Lake Llaviucu are published here for the first time and four ages are added to the four already published for Lake Fondococha (Schneider *et al.*, 2018). An additional ten ages were rejected; four were on bulk sediment and insect chitin (BE-3530.1.1, BE-3527.1.1, BE-3528.1.1, BE-3529.1.1). The bulk samples returned ages that are about 400-600 years older than indicated by the ages of terrestrial macrofossils measured in parallel samples, suggesting that the organic C had been stored on the landscape for centuries prior to entering the lake and thus the reservoir effect is not constant. Three of the rejected samples (BE-10953.1.1, BE-4779.1.1, BE-10956.1.1) were smaller than 0.1 mg dry mass and are therefore judged as unreliable. One returned a post-bomb spike age (BE-10954.1.1), one was from the near-surface where the ^{210}Pb age profile was used instead (BE-3518.1.1), and one was an outlier as determined by falling beyond the 95% confidence interval of the age-depth model (BE-4782.1.1). Age-depth models were also generated (not shown) using all the ages and the ages of the tephra layers were not substantially different, although the uncertainties were larger. Dating uncertainty was <±100 years (1 standard deviation) for samples larger than 0.2 mg dry mass but increased to >±200 years (1 standard deviation) for samples with mass <0.1 mg dry mass.
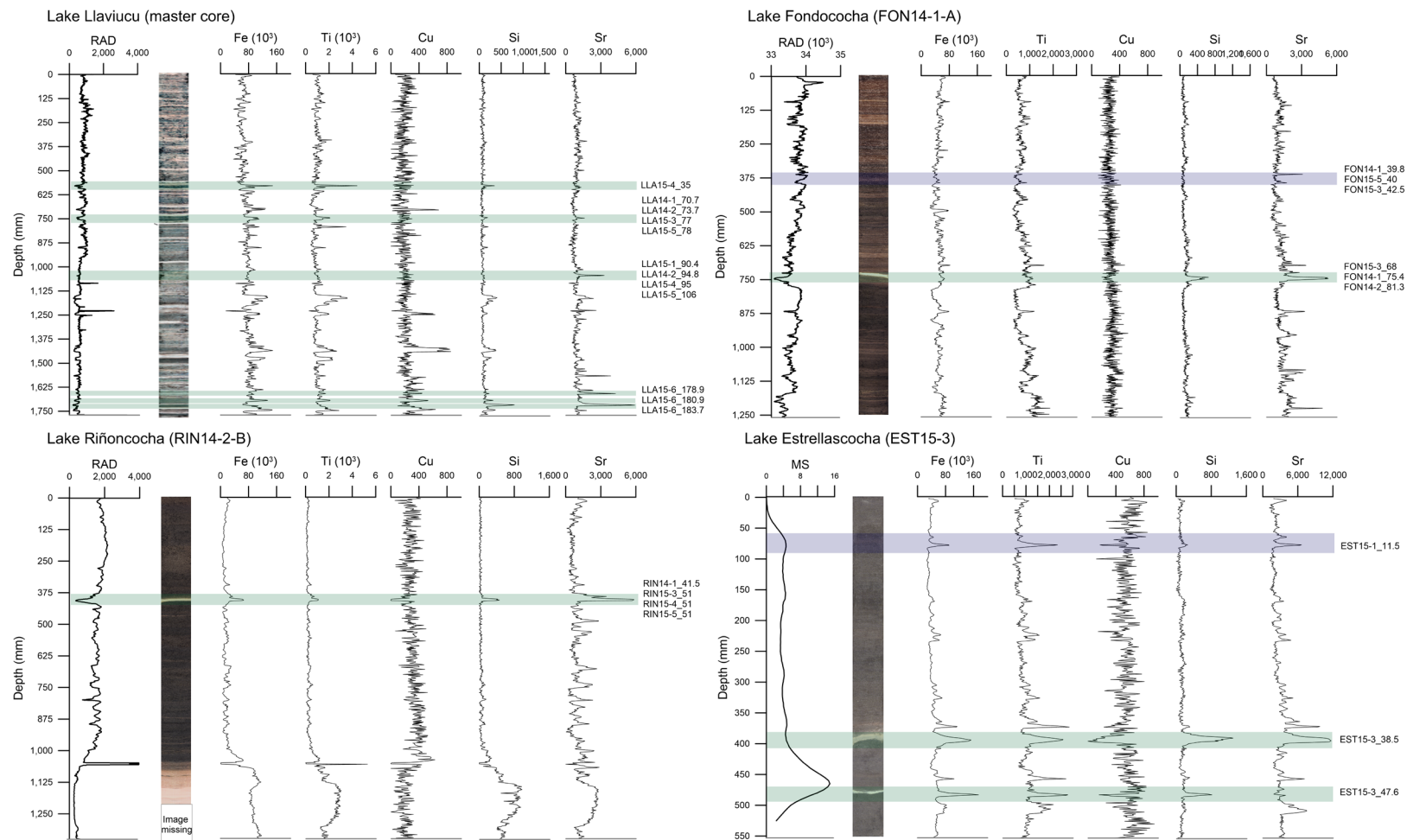
FIG. 2. Core images, MS (magnetic susceptibility), RAD (X-Radiography Density) and µXRF (micro X-Ray Fluorescence; Fe, Ti, Cu, Si, and Sr) counts presented for the four lake sediment cores. Investigated visible tephra and cryptotephra layers are highlighted in green and purple, respectively. Note the different vertical scales. LLA photo is colour-enhanced to increase contrast between background sediment and event layers. Tables containing XRF data can be found in supplementary Table S4. Also note that Lake Llaviucu layers identified in the figure are from three different cores whereas the core photo, RAD, and µXRF are from the composite core so have different depths.

TABLE 2. SUMMARY OF ANALYSED SAMPLES AND ¹⁴C DATA.

Core ID	LARA lab ID	Mid-point depth (cm)	Material	Sample mass (mg)	AMS source	¹⁴C a BP	Uncertainty (±1SD)	a cal BP (median)
LLA14-1-A*	BE-3518.1.1	21.15	*Isolepsis* and *Loricaria* fragments	0.405	gas	157	78	163
LLA14-1-A*	BE-3527.1.1	21.15	Bulk sediment	678.5	graphite	682	34	650
LLA14-1-A	BE-3519.1.1	55.45	*Loricaria* leaf fragments	2.804	graphite	317	22	387
LLA14-1-A*	BE-3528.1.1	55.45	Bulk sediment	868.6	graphite	891	22	804
LLA15-6	BE-4778.1.1	59.5	Wood and *Loricaria* fragments	0.648	graphite	332	44	392
LLA15-3*	BE-4779.1.1	61.6	Seed husk	0.065	gas	2,378	235	2,438
LLA14-1*	BE-10954.1.1	70	Unidentified	0.117	gas	-24	63	100
LLA15-3	BE-4780.1.1	71.5	*Loricaria* leaf fragment	0.027	gas	1,274	171	1,184
LLA14-1*	BE-10956.1.1	90	Grass and twig fragments	0.094	gas	2,239	85	2,233
LLA14-1	BE-10955.1.1	107.5	Bark and grass fragments	0.252	gas	1,781	68	1,704
LLA14-1-A*	BE-3529.1.1	108.5	Bulk sediment	891.5	graphite	2,248	23	2,227
LLA-15-6-II-A	BE-4781.1.1	180.5	Seed fragments	0.043	gas	2,923	356	3,109
FON14-2-I-B*	BE-3530.1.1	26.55	Bulk sediment	963	graphite	940	26	853
FON14-2-I-B	BE-3520.1.1	30	Seed; *Carex tricuspid*	0.195	gas	301	62	377
FON15-3	BE-4783.1.1	39.3	*Loricaria* leaf fragment	1.217	graphite	726	38	675
FON14-2-I	BE-10950.1.1	42.5	Periderm and grass fragment	0.095	gas	989	67	890
FON14-2-I*	BE-10953.1.1	53.5	Charred twig fragments	0.049	gas	1,943	99	1,893
FON15-3*	BE-4782.1.1	64.7	*Loricaria* leaf fragment	0.619	graphite	1,080	51	996
FON14-2-I	BE-10952.1.1	75.5	Charred twig fragments	0.347	graphite	2,104	50	2,079
FON14-2-I	BE-10951.1.1	92	Bark fragment	1.356	graphite	2,540	41	2,620

* Ages not included in the final chronologies.

The 185-cm-long sediment sequence from Lake Llaviucu extends back to *ca.* 3,000 a cal BP. Five of the 12 measured ¹⁴C ages were included in the age-depth models (Table 2). Sedimentation rates averaged over the entire core including event layers averages 0.58 and 0.62 mm/yr for the clam and rbacon age-depth models, respectively, with clam projecting an age of about 200 years older at the base of the core. Excluding the event layers results in average rates of 0.45 and 0.48 mm/yr in clam and rbacon, respectively. Both models indicate higher sedimentation over the last *ca.* 500 years, with average rates of *ca.* 1 mm/yr and peak values reaching 2.5 mm/yr in the last century. Between 500 and 900 a cal BP the rbacon model indicates lower sedimentation rates (*ca.* 0.3 mm/yr) than those observed in the
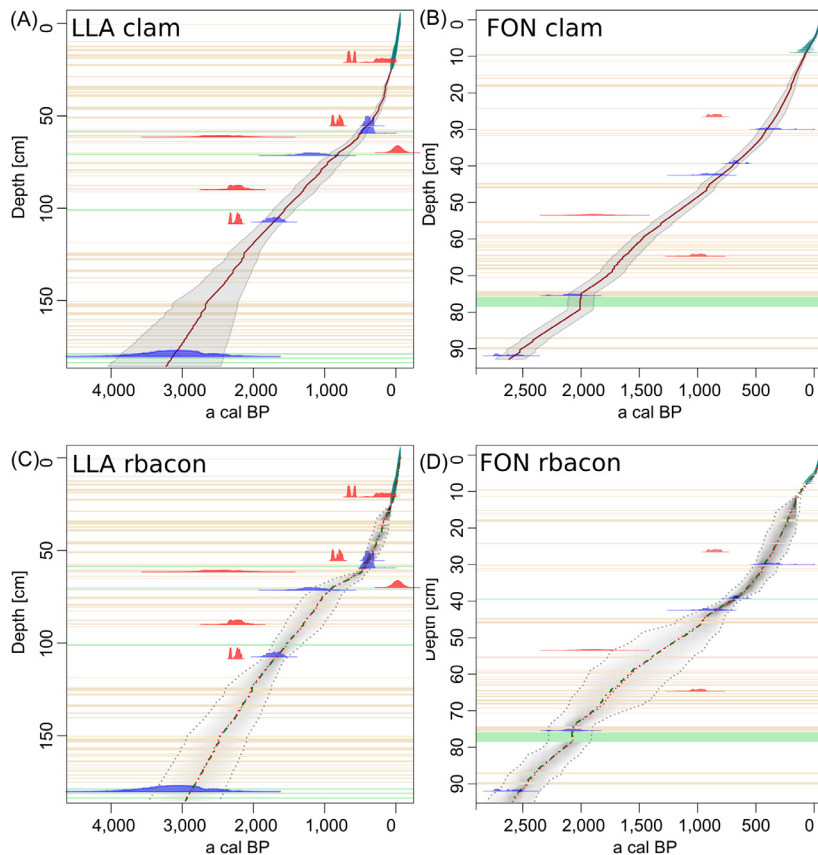
FIG. 3. Age-depth models for sediment cores from Lake Llaviucu (LLA, **A** and **C**), and Lake Fondococha (FON, **B** and **D**) comparing the output of clam (top row) and rbacon (bottom row) models, both with ^{210}Pb ages near the surface (green) and ^{14}C calibrated-age probability density curves (blue/red shapes). The ^{14}C dates on bulk sediment and insect chitin (red density curves) show substantial ^{14}C reservoir effects and were rejected. Event layers (orange horizontal bars) and tephra layers (green bars) are assumed to be deposited instantly. Model parameters are in supplementary Table S1; ^{14}C ages are in Table 2.

clam model. Prior to around 900 a cal BP, rbacon tends to model higher sedimentation rates than clam. This leads to the differences in the mean ages, but not in the range, modelled at 185 cm (rbacon: *ca*. 3,000 a cal BP; clam: *ca*. 3,200 a cal BP). The uncertainty ranges are better constrained in the top section of the core from Lake Llaviucu, which is mostly due to the higher ^{14}C-sample frequency. Interestingly, the clam model returns a larger age uncertainty range for the bottom *ca*. 35 cm and its spread tends to increase with increasing depth. The rbacon model on the other hand, shows comparably stable uncertainty ranges from *ca*. 110 to 185 cm.

The sediment core from Lake Fondococha extends back to *ca*. 2,600 a cal BP at 95 cm. Five of the eight measured ^{14}C ages were used to build the age-depth models (Table 2). Like Lake Llaviucu, the sedimentation rate also increases in the most recent period and reaches values between 0.7 and 1 mm/yr in the last century. Below 40 cm, both models show comparable and relatively stable sedimentation rates. Average sedimentation rates for both age-depth models are *ca*. 0.31 mm/yr, respectively, or 0.37 mm/yr when the rapidly deposited layers are included (Fig. 3A, C). The clam model returns overall lower uncertainty ranges than the rbacon model (135 versus 357 years, respectively, averaged over the core). The latter shows the largest range between *ca*. 45 cm and 75 cm, the longest core segment lacking acceptable ages. In contrast to Lake Llaviucu, the two age-depth modelling routines for Lake Fondococha produce similar ages. This can be explained with the narrower

calibrated-age probability distribution of the oldest ^{14}C sample in Lake Fondococha compared to the relatively wider distribution in Lake Llaviucu.

4.3. Tephra layer description

Twenty-nine macroscopically discreet and cryptotephra layers were analysed from the four lakes (Fig. 4). The tephra layers are typically light to medium grey and range in thickness from a few millimetres to 2 cm (Table 3). Typical tephra morphologies are dense to moderately vesiculated glass shard (Fig. 5), with high Sr, Si, MS and, at times, Fe and Ti abundances. RAD count values are often low reflecting dense material (high X-ray absorption, high RAD inferred density; Fig. 2). Whole-core MS was not particularly useful to detect cryptotephra due to its coarse resolution.

In Lake Llaviucu, six visible layers were identified at depths from 60-66 cm in the multiple cores (58.1 cm, composite core depth), 70-78 cm (71.3 cm), 90-106 cm (101.4 cm), 178.9 cm (179.2 cm), 180.9 cm (181.4 cm), and 183.7 cm (183.9 cm). Hereafter, tephra layer depths are cited according to their bottom depth in the composite cores. Tephra layer LLA_58.1 is medium to dark grey, composed of crystal fragments, pumice and dense glass shards. Tephra layer LLA_71.3 is light to dark grey, composed of crystal fragments and moderately vesicular glass shards. This tephra layer is distinguished by high Sr, Si, Ti, and Fe as well as by high RAD-inferred density. Tephra layer LLA_101.4 is mostly light grey, composed of crystal fragments, and dense glass shards. The proportion of crystal fragments is higher (~85%) in this layer than for others. This tephra layer is distinguished by high Sr counts. Tephra layer LLA_179.2 is medium grey, composed of crystal fragments and mostly dense glass shards. This tephra layer also generates high Sr counts. Tephra layer LLA_181.4 is medium to dark grey and mostly composed of pumice. This tephra layer is distinguished by high Si and Fe counts. Finally, layer LLA_183.9 is medium to dark grey and mostly composed of crystal fragments. This oldest tephra layer has high Sr and Si counts.

The ages of tephra layers in Lake Llaviucu range from 3.2 to 0.4 ka (Table 4). The age uncertainty is large (>±400 years) for the three oldest layers.
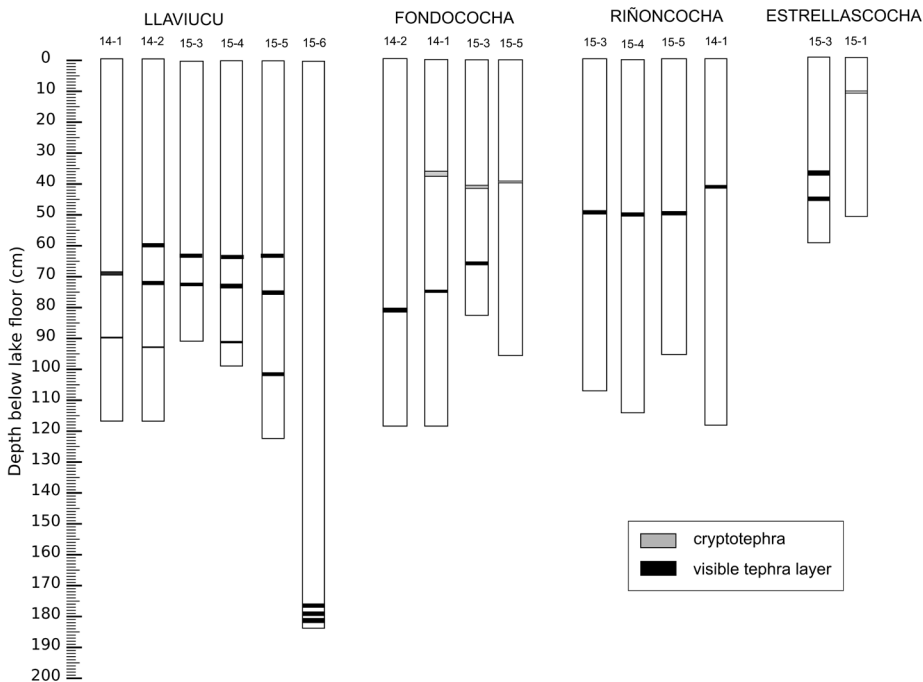

FIG. 4. Visible (black) and cryptotephra layers (grey) found in each of the sediment cores from four lakes arranged from lowest (Lake Llaviucu) to highest (Lake Estrellascocha) elevation.

TABLE 3. TEPHRA BED PHYSICAL CHARACTERISTICS.

Tephra layer ID*	Thickness (cm)	General colour	Componentry % (Crystal fragment/ glass shard/ pumice)	Glass shards description
LLA14-2_60.0	0.8	Light to dark grey	90/0/10	All dense
LLA15-3_64.0	1	Medium to dark grey	50/5/45	Mostly dense, few moderately vesiculated
LLA15-4_64.0	1	Medium to dark grey	50/5/45	Mostly dense, few moderately vesiculated
LLA15-5_66.0	1	Medium to dark grey	50/5/45	Mostly dense, few moderately vesiculated
LLA14-1_70.7	0.5	Medium grey	-	Mostly dense, some moderately vesiculated, few shards
LLA14-2_73.7	0.4	Medium grey	40/50/10	Mostly dense, some moderately vesiculated, few shards
LLA15-4_75.0	1	Light to dark grey	40/35/25	Mostly dense, some moderately vesiculated
LLA15-3_77.0	1	Light to dark grey	40/35/25	Mostly dense, some moderately vesiculated, few vesicular
LLA15-5_78.0	1	Light to dark grey	40/35/25	Mostly dense, some moderately vesiculated, few vesicular
LLA14-1_90.4	0.5	Light grey	-	All dense
LLA14-2_94.8	0.4	Light grey	75/0/25	All dense
LLA15-4_95.0	0.5	Light to dark grey	85/0/15	All dense
LLA15-5_106.0	1	Light to dark grey	85/0/15	All dense
LLA15-6_178.9	0.85	Medium grey	45/50/5	Mostly dense, some moderately vesiculated, some shards, few vesiculated
LLA15-6_180.9	1.2	Medium to dark grey	15/10/75	Mostly dense, some moderately vesiculated
LLA15-6_183.9	0.8	Medium to dark grey	60/35/5	Mostly dense, some shards, few vesiculated
FON14-1_39.8	1.3	Light to medium grey	15/85/0	Mostly moderately vesiculated, some dense, few vesicular, few shards
FON15-5_40.0	0.2	Light to dark grey	40/55/5	Mostly dense, some moderately vesiculated, few vesiculated, few shards
FON15-3_42.5	0.2	Light to dark grey	40/55/5	Mostly dense, some moderately vesiculated, few vesiculated, few shards
FON15-3_68.0	1	Light to dark grey	5/95/0	Mostly moderately vesiculated, some vesiculated, few shards, few dense
FON14-1_75.4	1.1		0/100/0	Mostly moderately vesiculated, some dense, some vesiculated
FON14-2_81.3	1	Light to medium grey	20/75/5	Mostly moderately vesiculated, some dense, few shards
RIN14-1_41.5	1.2	Light to dark grey	0/100/0	Mostly moderately vesiculated, few dense, few shards
RIN15-3_51.0	1	Light to dark grey	0/100/0	Mostly vesiculated, some moderately vesiculated
RIN15-4_51.0	1	Light to dark grey	0/100/0	Mostly vesiculated, some moderately vesiculated
RIN15-5_51.0	1	Light to dark grey	0/100/0	Mostly vesiculated, some moderately vesiculated
EST15-1_11.5	0.4	Dark grey	20/75/5	Mostly dense, few moderately vesiculated, few shards
EST15-3_38.5	1.4	Medium to dark grey	35/65/0	Some dense, some moderately vesiculated, few vesiculated glass
EST15-3_47.6	1	Light grey	0/100/0	Mostly dense, few shards

* Numbers at the end of the tephra layer IDs indicate the bottom depth of the tephra layers based on the composite cores. The three letters at the beginning of each tephra layer ID refers to the lake: **FON:** Fondococha; **LLA:** Llaviucu; **EST:** Estrellascocha; and **RIN:** Riñoncocha
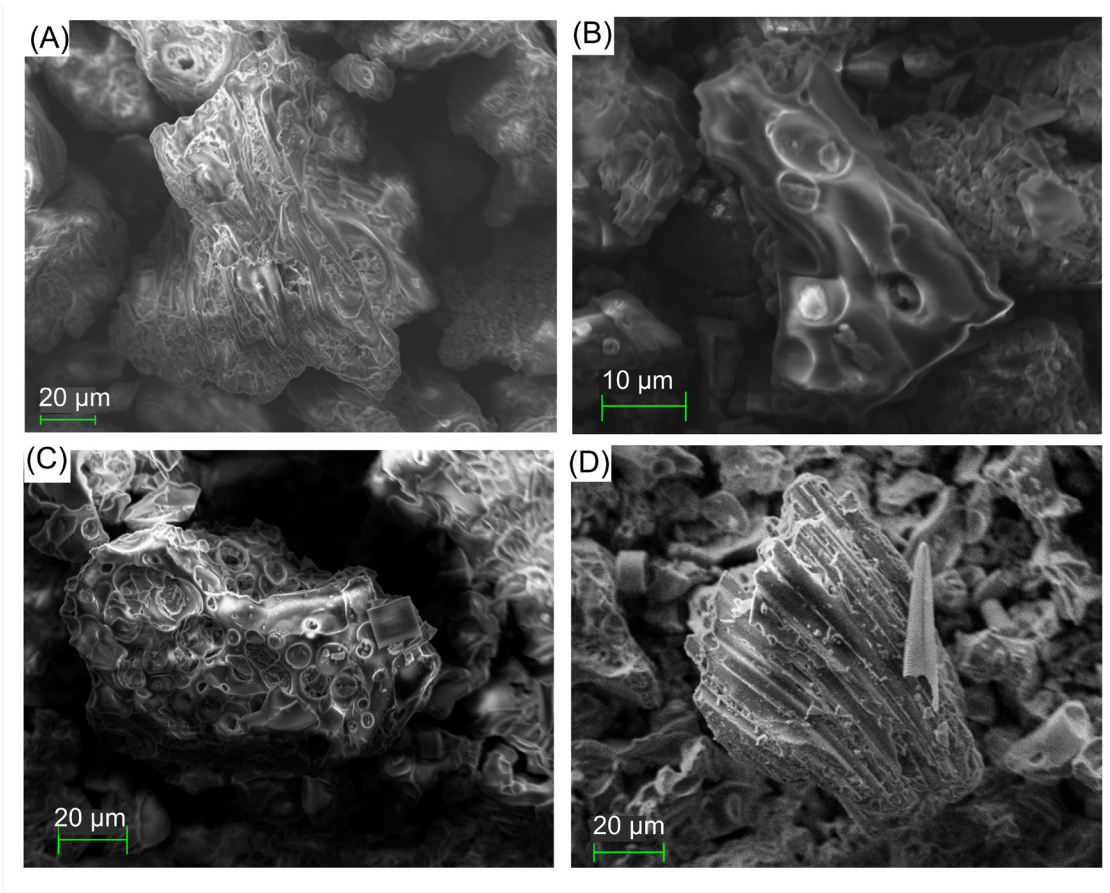
FIG. 5. Scanning electron micrographs of typical glass shards for **A.** Tephra layer LLA15-6_180.9 in Lake Llaviucu, **B.** Tephra layer FON14-1_39.8 in Lake Fondococha, **C.** Tephra layer RIN15-3_51 in Lake Riñoncocha, and **D.** Tephra layer EST15-3_38.5 in Lake Estrellascocha.

TABLE 4. TEPHRA LAYER BEST AGE ESTIMATES (a cal BP). BASED ON RBACON AND CLAM AGE-DEPTH MODELS.

Tephra layer ID*	Clam			Rbacon			Best age estimate**	±1SD
	Median	Min 95%	Max 95%	Median	Min	Max		
LLA_58.1	470	543	395	432	480	346	450	70
LLA_71.3	822	936	659	917	1,158	692	857	180
LLA_101.4	1,568	1,729	1,425	1,542	1,736	1,324	1,557	177
LLA_179.2	3,114	3,861	2,414	2,861	3,372	2,403	2,962	592
LLA_181.4	3,152	3,923	2,424	2,893	3,409	2,432	2,995	605
LLA_183.9	3,198	3,999	2,443	2,930	3,452	2,462	3,034	621
FON_39.8	698	762	659	687	780	626	694	63
FON_75.6	2,001	2,112	1,896	2,071	2,281	1,913	2,027	141

* Numbers at the end of the tephra layer ID indicate the composite depth (cm).
** Calculations in supplementary Table S2.

These layers are separated from each other by approximately 2 mm of sediment, implying an age difference of about 4 years based on the average sedimentation rate. The ages of the tephra layers differ little between clam and rbacon models.

In the sediment of Lake Fondococha, two tephra layers were found at depths 39.8-42.5 cm (39.8 cm, composite depth) and 68-81.3 cm (75.6 cm). Tephra layer FON_39.8 is light to dark grey, mostly composed of moderately vesiculated glass shards. This tephra layer has high Sr counts and high RAD-inferred density. Visible tephra layer FON_75.6 is light to dark grey and composed almost entirely of moderately vesiculated glass shards. This second tephra layer shows high Sr and Si counts as well as high RAD-inferred density. The choice of the age-depth model does not influence the assigned tephra layer ages.

In Lake Riñoncocha, one visible tephra layer was identified at 41.5-51.0 cm (41.5 cm based on core LLA14-1). Tephra layer RIN_41.5 is light to dark grey and entirely composed of vesiculated glass shards. This unique tephra layer is distinguished by high RAD-inferred density and high Sr, Si, Fe, and Ti counts. Insufficient organic material was available for a radiocarbon age determination from sediment immediately below this tephra layer.

Finally, in Lake Estrellascocha, three tephra layers were identified at depths of 11.5 cm, 38.5 cm, and 47.6 cm; in addition, several more cryptotephra layers may be present, but were not investigated in the present study (Fig. 2). Cryptotephra layer EST_11.5 is dark grey and mainly composed of dense glass shards. This layer shows high Sr, Si, Ti, and Fe counts as well as moderately high MS values. Visible tephra layer EST_38.5 is medium to dark grey with mostly moderately vesiculated glass shards. This second layer shows high Sr, Si, Ti, and Fe, and low Cu. Finally, visible tephra layer EST_47.6 is dark grey and entirely composed of dense glass shards. This third layer shows high Ti, Fe, and Si counts and high MS values.

In several instances, tephra beds were not present in every core from the same lake, although could have been present as an unexamined cryptotephra layer. For example, FON15-5 contained a single cryptotephra layer (FON15-5_40) and no visible layers even though core FON15-3, taken nearby, contained both (FON15-3_42.5 and FON15-3_68) (Fig. 4). Cryptotephra might be present but were not detected from each lake and from Lake Estrellascocha

(Fig. 2) in particular. For example, small peaks in Sr are visible for Lake Estrellascocha at depths where no cryptotephra layers were found (Fig. 2). Additionally, at least one bed appears to be present at only one site (e.g., EST15-1_11.5).

4.4. Tephra layer correlation

Tephra layers were correlated between Lakes Llaviucu and Fondococha based on their age-depth models. Various techniques were used to correlate tephra layers in the undated sediments of Lakes Riñoncocha and Estrellascocha. One layer is correlated between Lakes Llaviucu and Fondococha based on the overlap of their age (LLA_71.3 and FON_39.8, Table 4). Another correlation between those two lakes is made but is poorly constrained (LLA_101.4 and FON_75.6), and one more correlation to undated Lake Riñoncocha is based on PCA results conducted on the µXRF data (FON_75.6 and RIN_41.5, Fig. 6). The tephrochronology for all lakes is summarized in figure 7.

4.4.1. Tephra layer LLA_183.9 cm
This tephra layer was sampled from the sediment core of Lake Llaviucu (LLA15-6_183.9). The large uncertainty in the best age estimate for this tephra layer (3,034±621 a cal BP) precludes correlations with Lake Fondococha. Correlations to Lake Riñoncocha and Estrallascocha are not supported by elemental composition or componentry.

4.4.2. Tephra layer LLA_181.4 cm
This tephra layer was sampled from Lake Llaviucu (LLA15-6_180.9). Like the previous tephra layer, the large uncertainty in the best age estimate (2,995± 605 a cal BP) precludes correlations based on chronology. Sediment separates tephra layer LLA_183.7 from LLA_181.4 yet PCA indicates close similarity between the two layers (Fig. 6). Correlations to Lake Riñoncocha and Estrellascocha are not supported by elemental composition or componentry.

4.4.3. Tephra layer LLA_179.2 cm
Like the previous two tephra layers, this tephra layer was sampled from Lake Llaviucu sediment core (LLA15-6_178.9) and the large uncertainty in the best age estimate (2,962±592 a cal BP) also precludes possible correlations with tephra layers in Lake Fondococha. Sediment separates tephra layer
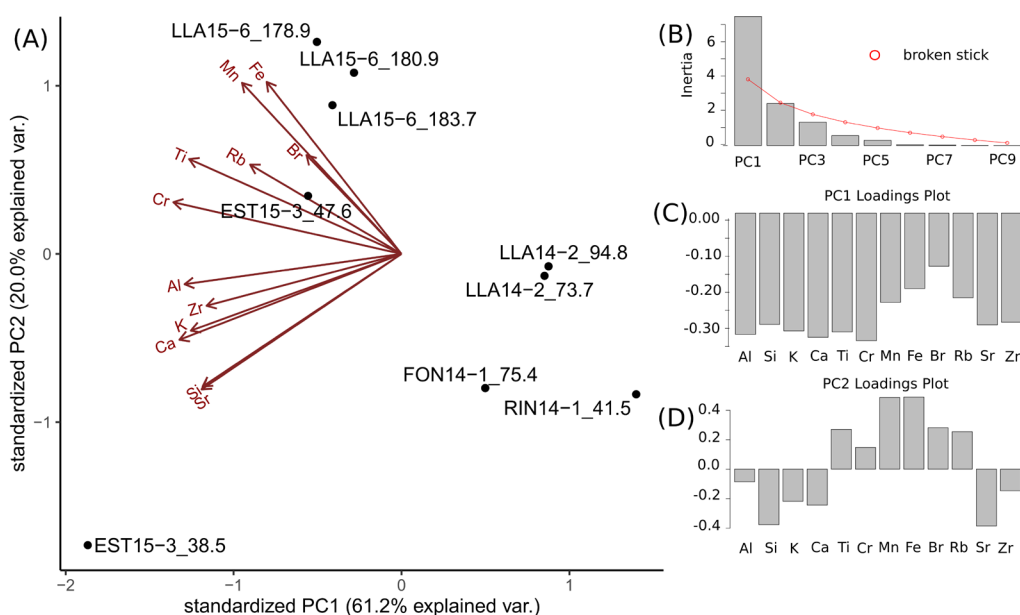
FIG. 6. **A.** Principal component analysis of μXRF data used to aid correlation of visible tephra beds among the lakes; **B.** The broken stick model indicates one significant principal component (PC): Standardized PC1 explains 62.1% of the geochemical variance and primarily distinguishes tephra samples based on (**C** and **D**) the loadings of elements Al to Zr.

LLA_181.4 from LLA_179.2 yet once again PCA indicates close similarity between layers LLA_181.4 and LLA_179.2 and layer LLA183.9. Furthermore, correlations to either Lake Riñoncocha or Lake Estrellascocha are not supported by elemental composition or componentry.

4.4.4. Tephra layer LLA_101.4 cm

The next tephra layer is sampled in four cores from Lake Llaviucu with a best age estimate of 1,557± 177 a cal BP. A tephra layer at the same stratigraphic location but with different elemental composition as seen from PCA (Fig. 6) is FON_75.6 found in three cores of Lake Fondococha. Both show high Sr levels (Fig. 2), although differ in Si. Their componentries are also different, with Lake Fondococha's tephra layers mostly composed of glass, whereas Lake Llaviucu's tephra layers are mostly crystal fragments (Table 3). Furthermore, the best age estimate for this tephra layer in Lake Fondococha does not overlap and is older (2,027±141 a cal BP). Considering the conflicting and inconclusive evidence, it is unclear whether tephra layer LLA_101.4 and FON_75.6 are the same. In contrast, confidence is higher for

the correlation of this tephra layer between Lake Fondococha and undated Lake Riñoncocha. Tephra layers FON_75.6 and RIN_41.5 are similar in elemental composition as seen from PCA (Fig. 6), componentry as well as colour (Table 3).

4.4.5. Tephra layer LLA_71.3 cm

Tephra layer LLA_71.3 is found in four cores from Lake Llaviucu, with a best age estimate of 857±180 a cal BP. Its age overlaps with the best age estimate of 694±63 a cal BP for Lake Fondococha's tephra layer FON_39.8. However, no other supporting evidence for this correlation exists. As the tephra layers in Lake Fondococha are cryptotephras, PCA analysis could not be applied. Tephra layer characteristics were variable, and correlations are made with low confidence. A best age estimate for this tephra layer using both lakes is 733±112 a cal BP. No evidence supports correlations to tephra layers found in either Lake Riñoncocha's or Lake Estrellascocha's sediment.

4.4.6. Tephra layer LLA_58.1 cm

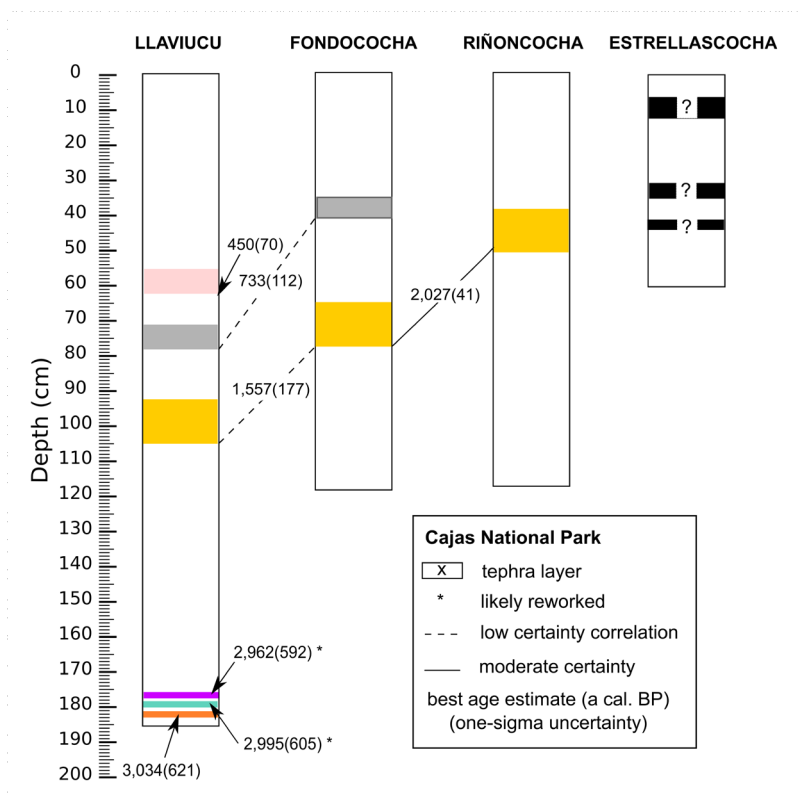The youngest dated tephra layer was sampled in three cores from Lake Llaviucu's sediment with a

FIG. 7. Simplified stratigraphic sequence showing depths below lake floor, thicknesses and correlations among tephra layers found in sediment cores from the four lakes. The best age estimates in a cal BP and the one sigma uncertainties (in brackets) calculated from the clam and rbacon age-depth models are shown. Note that the Llaviucu schematic represents the composite core.

best age estimate of 450±70 a cal BP. No evidence supports the correlation of this tephra layer to tephra layers detected in either Lake Riñoncocha or Lake Estrellascocha.

5. Discussion and conclusion

Lake sediments are generally reliable archives for catching and preserving tephra layers, and geographically distributed lakes are useful for documenting the extent of volcanic fallout (Lowe, 2011). However, from our results, some tephra layers appear to be missing from a few sites within the same lake, indicating that one core is not enough to confidently capture all the tephra falls. Heterogeneous areal distribution of tephra fallout deposition within a lake has been previously documented (Boygle, 1999; Kylander *et al.*, 2012; Pyne-O'Donnell, 2011). Although there is no obvious spatial pattern to the missing tephra layers, it is likely that currents

concentrate tephra in places on the lake floor, that wind recirculates tephra, and that sediment mixing can obliterate visual evidence of a tephra at some locations.

In addition, some lakes have captured more tephra fall events than others. Lake Llaviucu's sediment cores contain six tephra layers compared to two in Lake Fondococha and one in Lake Riñoncocha. However, it should be noted that Lake Llaviucu likely contains reworked tephra layers, as discussed below. Similar differences were highlighted by de Fontaine *et al.* (2007) who identified five times as many tephra layers in one lake 40 km away from another in south-central Alaska. Whereas the authors explained the differences through a host of catchment-basin and taphonomic reasons, it appears that catchment-to-lake area ratio is the property most likely affecting the variation seen in our study, with larger ratios associated with more frequent tephra beds. The delivery of tephra from the catchment into

the lake influences the tephra layer thickness. The greater number of tephra layers may be explained by Lake Llaviucu's much larger catchment-to-lake area ratio compared to the other lakes. Six tephra layers are found in Lake Llaviucu, with catchment-to-lake area ratio of 252, three in Lake Estrellascocha with a ratio of 12, two in Lake Fondococha with a ratio of 18, and one in Lake Riñoncocha with ratio of 6. Sedimentation rates unlikely play a role because they are similar in at least Lakes Fondococha and Llaviucu.

The presence of more tephra layers in Lake Llaviucu may also be explained by reworking of tephra from the catchment or within the lake decades after an eruption. Tephra layers LLA_178.9 and LLA_180.9 are candidate layers for reworking. Evidence for progressively more dilute glass concentration in LLA_178.9 and LLA_180.9 supports this hypothesis. Additionally, the sedimentary record of Lake Llaviucu contains many flood event layers, which combined with a large catchment, could rework tephra from the drainage basin over time through fluvial and runoff transport (Pyne-O'Donnell, 2011). Three consecutive eruptions (tephra layers LLA_183.9, LLA_180.9, and LLA_178.9) would be surprising but not unheard of. For example, Tungurahua is a highly active volcano that could have erupted three times in less than 100 years as evidenced by the eight eruptions during the documented 1999-2014 eruptive cycle (Bustillos *et al*., 2017). However, based on the sedimentation rate, only ~4 years separate the layers from each other and from the oldest layer, LLA_183.9, and would suggest specific and recurring wind directions. Finally, the similarity between the layers as seen from PCA could indicate reworking. Previous studies have demonstrated that layers of similar composition are likely to indicate reworking (Hopkins *et al*., 2015)

Both clam and rbacon models were calculated and compared to understand the strengths and disadvantages of the different age-depth models. The differences in the uncertainty ranges (shadings in Fig. 3) result from the different initial model parameters as well as the model calculations (Trachsel and Telford, 2017; Blaauw *et al*., 2018). Although the assumptions differ between models (Blaauw *et al*., 2018), the ages of tephra layers overlap even with average dating densities (one date per millennium). This can be attributed to ^{14}C ages that were taken from close to the tephra layers. The calculated best-age-

estimate further constrains the uncertainties native to individual age-depth modelling approaches. We therefore suggest that the presented tephra layer ages are relatively robust.

Up to now, one study has investigated tephra fallout in southern Ecuador during the Holocene, but found no prominent tephra layers in the past 2,000 years (Rodbell *et al*., 2002). This led the authors to suggest that wind trajectories had shifted. However, our discovery of possibly three tephra layers during this interval (two if LLA_101.4 and FON_75.6 are the same) and one more around 3,000 a cal BP, with one of the five traceable across at least two sites, indicates that wind conditions were likely not much different in the late Holocene. The lack of tephra layers in the previous study can likely be attributed to focusing on one core per lake or the lack of methodology suitable to detect cryptotephra and underscores our conclusion that more than one core is needed to fully account for tephra fallout events.

Nevertheless, Rodbell *et al*. (2002) identified two tephra layers (G and F, in their Fig. 3) in Lakes Pallcacocha, Chorreras, and Llaviucu that could correlate with the tephra layers described in our study. Tephra layers G and F in Lake Pallcacocha may correspond to FON_75.6 in terms of age but may be older than LLA_101.4. Based on their ages, tephra layers G and F in Lake Chorreras may correspond to two of the oldest three tephra layers in Lake Llaviucu, either LLA_183.9, LLA_181.4 or LLA_179.2. In detail, the age ascribed to tephra layer G (3,380+60, -100 a cal BP, Rodbell *et al*., 2002) falls within the age range of all three oldest Lake Llaviucu tephra layers and within the age range of the Tungurahua eruption described by Le Pennec *et al*. (2013) (*ca*. 3,050 a cal BP). However, evidence suggests that two of the three oldest Lake Llaviucu layers (LLA_181.4 and LLA_179.2) may be reworked.

Correlations with known eruptions were attempted using estimated tephra layer age. Until further evidence is available, only LLA_183.9 of the three oldest Llaviucu layers is considered as a primary tephra. Tungurahua (volcano 4 in Fig. 1) erupted *ca*. 3,000 a cal BP, initiating two lahars and causing disruption of local communities (Hall *et al*., 1999; Le Pennec *et al*., 2012, 2013). It is likely that the oldest tephra layer found in Lake Llaviucu's sediment (LLA_183.9) represents one eruption from Tungurahua (Table 5).

The next two tephra layers, FON_75.6 and LLA_101.4, are inconclusively correlated, and

TABLE 5. BEST AGE ESTIMATES AND CANDIDATE ERUPTION EVENTS FOR FOUR TEPHRA LAYERS FROM CAJAS NATIONAL PARK.

Tephra layer ID	Best age estimate		Candidate volcano(es)†	Eruption (a cal BP)	References
	a cal BP	±1SD			
LLA_58.1	450	70	Cotopaxi[2]	418[§]	Barberi *et al*. (1995)
LLA_71.3	733	112	Tungurahua[4]	605±32*	Le Pennec *et al*. (2008)
			Quilotoa[1]	~800	Mothes and Hall (2008)
LLA_101.4	1,557	177	Tungurahua[4]	1,483*	Venzke (2016)
			Cotopaxi[2]	1,510±212*	Venzke (2016)
			Chimborazo[3]	1,530±50	Barba *et al*. (2008)
FON_75.6	2,027	41	Tungurahua[4]	2,020*	Venzke (2016)
			Cotopaxi[2]	2,023±107*	Barberi *et al*. (1995)
LLA_183.9	3,034	621	Tungurahua[4]	3,117±124*	Hall *et al*. (1999)

* Ages calibrated from the originally reported uncalibrated ages.
§ Historical account.
† Superscript number represents volcano ID in figure 1.

might have been erupted from different sources. The age of tephra layer FON_75.6 (2,027±41 a cal BP) overlaps with the age of large eruptions from Tungurahua (volcano 4 in Fig. 1; Venzke, 2016) and from Cotopaxi (volcano 2 in Fig. 1; Barberi *et al*., 1995) (Table 5). Similarly, the age of LLA_101.4 overlaps with other eruptions from the same two volcanoes (Venzke, 2016). Additionally, LLA_101.4 could correspond to an eruption from Chimborazo (volcano 3 in Fig. 1) (Barba *et al*., 2008). Few records of eruptions from Sangay, the closest volcano to CNP, exist prior to 500 a cal BP making this volcano another candidate. A tephra layer of similar age (1,470 a cal BP) in Lake Baños was attributed to the volcano Antisana (Matthews-Bird *et al*., 2017) but both are located in northern Ecuador at a significant distance from CNP. Considering the distance between the lakes and the volcanoes, it is most likely that the tephra layers represent eruptions from Tungurahua.

The age of the next dated tephra layer, LLA_71.3 at 733±112 a cal BP, overlaps with two known eruptions. The first is from the devastating Quilotoa (volcano 1 in Fig. 1) eruption *ca*. 800 a cal BP, likened in scale to the 1991 Pinatubo eruption (Mothes and Hall, 1998, 2008). Tephra fallout from that eruption was found *ca*. 160 km south from the vent (Mothes and Hall, 2008), suggesting ash could have reached CNP. Ash from this eruption was possibly found in Laguna Pindo, 112 km east of Quilotoa (Matthews-Bird *et al*., 2017). The second is from Tungurahua during an active period *ca*. 600 a cal BP (Le Pennec *et al*., 2008). Both volcanoes are a similar distance away from the lakes. Ash fallout from Tungurahua was modelled to have reached as far south as CNP during eruptions in 1999 and 2001 (Le Pennec et tephra erual., 2012), but evidence for these particular eruptions has not been found in the lake sediment. Although several source volcanoes have been mentioned, all tephra layers previously discussed can be attributed to eruptions from one nearby volcano, Tungurahua.

Finally, and unlike the others, tephra layer LLA_58.1 (450±70 a cal BP) best matches the historical Cotopaxi eruption of 418 a cal BP (Table 5) (Barberi *et al*., 1995). No Tungurahua eruption has been recorded around that time. However, insufficient evidence is available from our study to suggest this tephra layer has a different elemental composition from the tephra layers previously described. The four or five layers identified provide additional information on eruption magnitude and wind direction. Although the thickness of a tephra layer is not always correlated with the magnitude of an eruption because plume trajectories vary among eruptions, the new results add to the knowledge of the extent and volume of tephra deposition during different eruptions. Previous

research suggested that volcanic ash did not reach CNP during the Late Holocene, implying a change in wind direction, a decrease in eruption magnitude, or both (Rodbell *et al.*, 2002). Here we demonstrate that eruption magnitude, wind direction or both have likely not changed substantially during the last 2,000 years as compared to the Late Glacial. This suggests that volcanic eruptions will likely remain a hazard for southern Ecuador, where tephra has fallen on average every ~500 years at a minimum and likely more frequently.

In conclusion, five tephra layers were identified from 29 visible and cryptotephra layers preserved in multiple sediment cores from four lakes in CNP. Chronologies were developed from two of the lakes and one tephra layer could be correlated based on age. Correlations with the other two lakes were based on elemental composition, colour, and componentry. Tephra layer LLA_183.9 was followed by two reworking events, LLA_181.4, and LLA_179.2, closely spaced in time (3,034±621, 2,995±605, and 2,962±592 a cal BP, respectively) as preserved in Lake Llaviucu. These are followed by tephra layers LLA_101.4 and FON_75.6 (1,557±177 and 2,027±41 a cal BP, respectively), that due to age uncertainty and limited physical evidence, cannot be unambiguously attributed to the same eruption. Tephra layer LLA_71.3 (733±112 a cal BP) is correlated across two lakes. Tephra LLA_58.1 (450±70 a cal BP) is only found in Lake Llaviucu. Three tephra layers were also found in Lake Estrellascocha but could not be correlated.

The first study in this region provided a starting point but had not found any events during the last 2,000 years likely because that study focused on thick layers in only one core (Rodbell *et al.*, 2002). Here we document probably three events over the last 2,000 years. As evidenced from our study, some tephra layers appeared to be missing from one of the cores of the depocenters, and some lakes recorded more events than others, leading us to conclude, like previous work before us, that one core or one lake is not enough to confidently capture all the tephra layers from surrounding volcanoes (*e.g.*, Boygle, 1999; Kaufman *et al.*, 2012). Additionally, a systematic search using emerging cryptotephra techniques (Davies, 2015), which was not performed in this study, should yield evidence for even more events. The addition of four or five marker events is a significant contribution for future studies of lake sediments in Cajas National Park where radiocarbon dating is often challenging. While a systematic survey of lakes in southern Ecuador would be needed to produce a history of eruption frequency, the presence and abundance of tephra layers during the Late Holocene indicate that volcanic eruptions are a greater hazard to southern Ecuador than previously reported.

Declarations of competing interest

The authors declare that they have no known competing financial interests or personal relationships that could have appeared to influence the work reported in this paper.

Data availability

The data and calculations presented in this manuscript are uploaded online at https://boris.unibe.ch/146277/ (BORIS, Uni Bern) (last visit 03/09/2020).

References

Alloway, B.V.; Lowe, D.J.; Larsen, G.; Shane, P.A.R.; Westgate, J.A. 2013. Tephrochronology. Encyclopedia of Quaternary Science: 277-304.

Bandowe, B.A.M.; Fränkl, L.; Grosjean, M.; Tylmann, W.; Mosquera, P.V.; Hampel, H.; Schneider, T. 2018. A 150-year record of polycyclic aromatic compound (PAC) deposition from high Andean Cajas National Park, southern Ecuador. Science of the Total Environment 621: 1652-1663. doi: 10.1016/j.scitotenv.2017.10.060.

Barba, D.; Robin, C.; Samaniego, P.; Eissen, J.P. 2008. Holocene recurrent explosive activity at Chimborazo

volcano (Ecuador). Journal of Volcanology and Geothermal Research 176: 27-35.

Barberi, F.; Coltelli, M.; Frullani, A.; Rosi, M.; Almeida, E. 1995. Chronology and dispersal characteristics of recently (last 5000 years) erupted tephra of Cotopaxi (Ecuador): implications for long-term eruptive forecasting. Journal of Volcanology and Geothermal Research 69: 217-239. doi: 10.1016/0377-0273(95)00017-8.

Blaauw, M. 2019. Clam: Classical age-depth modelling of cores from deposits. R package version 2.3.2. https://CRAN.R-project.org/package=clam (last visit 03/09/2020).

Blaauw, M.; Christen, J.A. 2019. Rbacon: Age-depth modelling using bayesian statistics. R package version 2.3.9.1. https://CRAN.R- project.org/package=rbacon. (last visit 03/09/2020).

Blaauw, M.; Christen, J.A.; Bennett, K.D.; Reimer, P.J. 2018. Double the dates and go for Bayes-Impacts of model choice, dating density and quality on chronologies. Quaternary Science Reviews 188: 58-66.

Boygle, J. 1999. Variability of tephra in lake and catchment sediments, Svínavatn, Iceland. Global Planetary Change 21: 129-149. doi: 10.1016/j.quascirev.2018.03.032.

Bustillos, J.; Romero, J.E.; Guevara, A.; Díaz-Alvarado, J. 2018. Tephra fallout from the long-lasting Tungurahua eruptive cycle (1999-2014): Variations through eruptive style transition and deposition processes. Andean Geology 45 (1): 47-77. doi: 10.5027/andgeoV45n1-3036.

Butz, C.; Grosjean, M.; Fischer, D.; Wunderle, S.; Tylmann, W; Rein, B. 2015. Hyperspectral imaging spectroscopy: a promising method for the biogeochemical analysis of lake sediments. Journal of Applied Remote Sensing 9: 1-20. doi:10.1117/1.JRS.9.096031.

Buytaert, W.; Deckers, J.; Wyseure, G. 2006. Description and classification of nonallophanic Andosols in south Ecuadorian alpine grasslands (páramo). Geomorphology 73: 207-221. doi: 10.1016/j.geomorph.2005.06.012.

Croudace, I.W.; Rindby, A.; Rothwell, R.G. 2006. ITRAX: description and evaluation of a new multi-function X-ray core scanner. *In* New Techniques in Sediment Core Analysis (Rothwell, R.G.; editor). Geological Society of London: 677-695. London.

Davies, S.M. 2015. Cryptotephras: the revolution in correlation and precision dating. Journal of Quaternary Science 30 (2): 114-130. doi: 10.1002/jqs.2766.

De Fontaine, C.S.; Kaufman, D.S.; Scott Anderson, R.; Werner, A.; Waythomas, C.F.; Brown, T.A. 2007. Late Quaternary distal tephra-fall deposits in lacustrine sediments, Kenai Peninsula, Alaska. Quaternary Research 68: 64-78.

Garrison, J.M.; Davidson, J.P.; Hall, M.; Mothes, P. 2011. Geochemistry and petrology of the most recent deposits from Cotopaxi Volcano, Northern Volcanic Zone, Ecuador. Journal of Petrology 52 (9): 1641-1678. doi: 10.1093/petrology/egr023.

Geyh, M.A.; Grosjean, M.; Núñez, L.; Schotterer, U. 1999. Radiocarbon reservoir effect and the timing of the late-glacial/early Holocene humid phase in the Atacama Desert (Northern Chile). Quaternary Research 52 (2): 143-153. doi: 10.1006/qres.1999.2060.

Hall, M.L.; Robin, C.; Beate, B.; Mothes, P.; Monzier, M. 1999. Tungurahua Volcano, Ecuador: structure, eruptive history and hazards. Journal of Volcanology and Geothermal Research 91: 1-21.

Hall, M.L.; Samaniego, P.; Le Pennec, J.L.; Johnson, J.B. 2008. Ecuadorian Andes volcanism: A review of Late Pliocene to present activity. Journal of Volcanology and Geothermal Research 176: 1-6.

Harden, C.P. 2006. Human impacts on headwater fluvial systems in the northern and central Andes. Geomorphology 79: 249-263. doi: 10.1016/j.geomorph.2006.06.021

Hidalgo, S.; Monzier, M.; Almeida, E.; Chazot, G.; Eissen, J.P.; van der Plicht, J.; Hall, M.L. 2008. Late Pleistocene and Holocene activity of the Atacazo-Ninahuilca Volcanic Complex (Ecuador). Journal of Volcanology and Geothermal Research 176: 16-26.

Hopkins, J.L.; Millet, M.-A.; Timm, C.; Wilson, C.J.N.; Leonard, G.S.; Palin, J.M.; Neil, H. 2015. Tools and techniques for developing tephra stratigraphies in lake cores: A case study from the basaltic Auckland Volcanic Field, New Zealand. Quaternary Science Reviews 123: 58-75. doi: 10.1016/j.quascirev.2015.06.014.

Kaufman, D.S.; Jensen, B.J.L.; Reyes, A.V.; Schiff, C.J.; Froese, D.G.; Pearce, N.J.G. 2012. Late Quaternary tephros-tratigraphy, Ahklun Mountains, SW Alaska. Journal of Quaternary Science 27: 344-359. doi: 10.1002/jqs.1552.

Kylander, M.E.; Lind, E.M.; Wastegard, S.; Lowemark, L. 2012. Recommendations for using XRF core scanning as a tool in tephrochronology. The Holocene 22: 371-375. doi: 10.1177/0959683611423688.

Le Pennec, J.; Jaya, D.; Samaniego, P.; Ramón, P.; Yánez, S.M.; Egred, J.; Plicht, J.; Van Der. 2008. The AD 1300-1700 eruptive periods at Tungurahua volcano, Ecuador, revealed by historical narratives, stratigraphy and radiocarbon dating. Journal of Volcanology and Geothermal Research 176: 70-81.

Le Pennec, J.L.; Ruiz, G.A.; Ramón, P.; Palacios, E.; Mothes, P.; Yepes, H. 2012. Impact of tephra falls on Andean communities: The influences of eruption size and weather conditions during the 1999-2001 activity of

Tungurahua volcano, Ecuador. Journal of Volcanology and Geothermal Research 217-218: 91-103.

Le Pennec, J.L.; De Saulieu, G.; Samaniego, P.; Jaya, D.; Gailler, L. 2013. A devastating Plinian eruption at Tungurahua volcano reveals Formative occupation at ~1100 cal BC in central Ecuador. Radiocarbon 55: 1199-1214.

Liu, E.J.; Oliva, M.; Antoniades, D.; Giralt, S.; Granados, I.; Pla-Rabes, S.; Toro, M.; Geyer, A. 2016. Expanding the tephrostratigraphical framework for the South Shetland Islands, Antarctica, by combining compositional and textural tephra characterisation. Sedimentary Geology 340: 49-61. doi: 10.1016/j.sedgeo.2015.08.002.

Lowe, D.J. 2011. Tephrochronology and its application: A review. Quaternary Geochronology 6: 107-153.

Marsh, E.J.; Bruno, M.C.; Fritz, S.C.; Baker, P.; Capriles, J.M.; Hastorf, C.A.; 2018. IntCal, SHCal, or a Mixed Curve? Choosing a ^{14}C Calibration Curve for Archaeological and Paleoenvironmental Records from Tropical South America. Radiocarbon 60: 925-940.

Matthews-Bird, F.; Brooks, S.J.; Gosling, W.D.; Gulliver, P.; Mothes, P.; Montoya, E. 2017. Aquatic community response to volcanic eruptions on the Ecuadorian Andean flank: evidence from the palaeoecological record. Journal of Paleolimnology 58: 437-453.

Monzier, M.; Robin, C.; Samaniego, P.; Hall, M.L.; Cotten, J.; Mothes, P.; Arnaud, N. 1999. Sangay volcano, Ecuador: structural development, present activity and petrology. Journal of Volcanology and Geothermal Research 90: 49-79.

Mosquera, P.V.; Hampel, H.; Vázquez, R.F.; Alonso, M.; Catalán, J. 2017. Abundance and morphometry changes across the high-mountain lake-size gradient in the tropical Andes of Southern Ecuador. Water Resources Research 53: 7269-7280.

Mothes, P.A.; Hall, M.L. 1998. Quilotoa's 800 y BP ash: a valuable stratigraphicmarker unit for the integration period. *In* Actividad Volcánica y Pueblos Precolombinos en el Ecuador (Mothes, P.; editor), Abya-Yala: 111-138. Quito.

Mothes, P.A.; Hall, M.L. 2008. The Plinian fallout associated with Quilotoa's 800 yr BP eruption, Ecuadorian Andes. Journal of Volcanology and Geothermal Research 176: 56-69.

Paladines, A.; Guzmán, J. 1980. Mapa geológico del Ecuador. Dirección General de Geología y Minas, Hoja Geológica de Cuenca. Escala 1:100,000. Quito.

Peti, L.; Gadd, P.S.; Hopkins, J.L.; Augustinus, P.C. 2019. Itrax μ-XRF core scanning for rapid tephrostratigraphic analysis: a case study from the Auckland Volcanic Field maar lakes. Journal of Quaternary Science: 1-12.

Pyne-O'Donnell, S. 2011. The taphonomy of Last Glacial-Interglacial Transition (LGIT) distal volcanic ash in small Scottish lakes. Boreas 40: 131-145

R Core Team. 2019. R: A language and environment for statistical computing. R Foundation for Statistical Computing, Vienna, Austria. https://www.R-project.org/. (last visit 03/09/2020).

Reimer, P.; Bard, E.; Bayliss, A.; Beck, J.W.; Blackwell, P.G.; Bronk Ramsey, C.; Buck, C.E.; Cheng, H.; Edwards, R.L.; Friedrich, M.; Grootes, P.M.; Guilderson, T.P.; Haflidason, H.; Hajdas, I.; Hatté, C.; Heaton, T.J.; Hoffman, D.L.; Hogg, A.G.; Hughen, K.A.; Kaiser, K.F.; Kromer, B.; Manning, S.W.; Niu, M.; Reimer, R.W.; Richards, D.A.; Scott, E.M.; Southon, J.R.; Staff, R.A.; Turney, C.S.M.; Van der Plicht, J. 2013. IntCal13 and Marine13 radiocarbon age calibration curves 0-50,000 years cal. BP. Radiocarbon 55: 1869-1887.

Rodbell, D.T.; Bagnato, S.; Nebolini, J.C.; Seltzer, G.O.; Abbott, M.B. 2002. A Late Glacial-Holocene Tephrochronology for Glacial Lakes in Southern Ecuador. Quaternary Research 57: 343-354.

Rodbell, D.T.; Seltzer, G.O.; Mark, B.G.; Smith, J.A.; Abbott, M.B. 2008. Clastic sediment flux to tropical Andean lakes: records of glaciation and soil erosion. Quaternary Science Reviews 27: 1612-1626.

Salazar, G.; Zhang, Y.L.; Agrios, K.; Szidat, S. 2015. Development of a method for fast and automatic radiocarbon measurement of aerosol samples by online coupling of an elemental analyzer with a MICADAS AMS. Nuclear Instruments and Methods in Physics Research, Section B: Beam Interactions with Materials and Atoms 361: 163-167.

Schneider, T.; Hampel, H.; Mosquera, P.V.; Tylmann, W.; Grosjean, M. 2018. Paleo-ENSO revisited: Ecuadorian Lake Pallcacocha does not reveal a conclusive El Niño signal. Global Planetary Change 168: 54-66.

Schnurrenberger, D.; Russell, J.; Kelts, K. 2003. Classification of lacustrine sediments based on sedimentary components. Journal of Paleolimnology 29: 41-154.

Schultheiss, P.J.; Weaver, P.P.E. 1992. Multi-sensor core logging for science and industry. *In* Institute of Electric and Electronic Engineering, Oceans 92: 608-613. New York.

Shane, P. 2000. Tephrochronology: A New Zealand case study. Erth Science Reviews 49: 223-259.

Szidat, S.; Salazar, G.A.; Vogel, E.; Battaglia, M.; Wacker, L.; Synal, H.-A.; Türler, A. 2014. ^{14}C analysis and sample preparation at the new Bern laboratory for the analysis of radiocarbon with AMS (LARA). Radiocarbon 56: 561-566. doi: 10.2458/56.17457.

Trachsel, M.; Telford, R.J. 2017. All age-depth models are wrong, but are getting better. The Holocene 27: 860-869.

Van Colen, W.R.; Mosquera, P.; Vanderstukken, M.; Goiris, K.; Carrasco, M.C.; Decaestecker, E.; Alonso, M.; León-Tamariz, F.; Muylaert, K. 2017. Limnology and trophic status of glacial lakes in the tropical Andes (Cajas National Park, Ecuador). Freshwater Biology 62 (3): 458-473. doi: 10.1111/fwb.12878.

Venzke, E. 2016. Global volcanism program. Volcanoes World, v. 4.8.4. Smithsonian Institution, http://volcano.si.edu/gvp_votw.cfm. (last visit 03/09/2020).

Vogel, H.; Zanchetta, G.; Sulpizio, R.; Wagner, B.; Nowaczyk, N. 2010. A tephrostratigraphic record for the last glacial-interglacial cycle from Lake Ohrid, Albania and Macedonia. Journal of Quaternary Science 25: 320-338.

Zawalna-geer, A.; Lindsay, J.A.N.M.; Davies, S.; Augustinus, P.; Davies, S. 2016. Extracting a primary Holocene crytoptephra record from Pupuke maar sediments, Auckland, New Zealand. Journal of Quaternary Science 31 (5): 442-457. doi: 10.1002/jqs.2866.